Lawrence Berkeley National Laboratory
LBL Publications

Title
Boreal carbon loss due to poleward shift in low-carbon ecosystems

Permalink
https://escholarship.org/uc/item/4cm2g7sx

Author
Koven, C.D.

Publication Date
2013-04-01

Boreal carbon loss due to poleward shift in low-carbon ecosystems

Charles D. Koven

Climate change can be thought of in terms of geographical shifts in climate properties. Examples include assessments of shifts in habitat distributions[1], of the movement needed to maintain constant temperature or precipitation[2], and of the emergence and disappearance of climate zones[3]. Here I track the movement of analogue climates within climate models. From the model simulations, I define a set of vectors that link a historical reference climate for each location to the location in a changed climate whose seasonal temperature and precipitation cycles best match the reference climate. I use these vectors to calculate the change in vegetation carbon storage with climate change due to ecosystems following climate analogues. Comparing the derived carbon content change to direct carbon projections by coupled carbon–climate models reveals two regions of divergence. In the tropical forests, vector projections are fundamentally uncertain because of a lack of close climatic analogues. In the southern boreal forest, carbon losses are projected in the vector perspective because low-carbon ecosystems shift polewards. However, the majority of carbon–climate models—typically without explicit simulation of the disturbance and mortality processes behind such shifts—instead project vegetation carbon gains throughout the boreal region. Southern boreal carbon loss as a result of ecosystem shift is likely to offset carbon gains from northern boreal forest expansion.

Earth's surface is composed of a diverse mosaic of climates, whose range exceeds the expected mean changes to climate over the near future. Because different ecosystems span Earth's range of climates, an expected outcome of climate change is a geographic shift in ecosystem boundaries as new regions become habitable and parts of former ranges become uninhabitable for different species[1]. One way of considering such shifts is as a velocity at which ecosystems must move to maintain a given climate variable, which can be calculated as the ratio of the time rate of change and the spatial gradient[2]. However, different climate variables will have different gradients in both space and time, and thus velocities will differ in both direction and magnitude between variables such as temperature and precipitation[4,5].

The climate analogue approach[3,6], of tracking in space the most statistically similar climate over an interval of time, may answer questions of where a given historical climate is going to, and where a given future climate will be coming from. Thus a climate analogue velocity can be defined as the spatial vector connecting reference and closest analogue climates divided by the time interval. This combines information from multiple climate variables, and facilitates consideration of where the climate velocity concept fails by assessing how similar the analogue climate is to the original. Using a set of global climate models, and at the resolution of each

model, this climate analogue velocity is calculated at each gridcell, defining a set of vectors and associated dissimilarity (Fig. 1). Here the climate variables used are 24 monthly mean values, 12 each of temperature and precipitation, and they are weighted by the inverse of interannual variability. Using fixed monthly values includes seasonality effects, but does not allow for relative changes in seasonal phasing to offset shifts for example, tropical ecosystems finding close but differently phased analogues in the opposite hemisphere. As each individual species will have their own specific tolerances and sensitivities, other combinations and approaches to weighting variables are possible[5].

The vectors can be calculated in the forward direction, by finding the future gridcell that best matches a given historical gridcell, to show where a given historical climate would be going to in the future. Alternately, they can be calculated in the reverse direction, by finding the historical gridcell that best matches a given future gridcell, to find where a given future climate would be coming from. Here I use data at the resolution of individual model gridcells; therefore sub-gridscale variability is neglected and vectors represent movement at the gridcell scale. Thus the pattern differs qualitatively from climate velocity calculated using high-resolution data, particularly where fine-scale elevation gradients exist that serve to reduce climate velocity by allowing change along local elevation gradients[2].

The direction of vectors in Fig. 1 is consistent with the expectation that ecosystems will shift poleward (in extratropics) and uphill (in tropics), while maintaining continentality, to accommodate global warming. Temperature exerts a stronger influence than precipitation in this analysis (Supplementary Figs S1 and S2), because temperature change is larger relative to both interannual variability and spatial gradients. The direction and magnitude of vectors for the forward and reverse directions in Fig. 1a and c are consistent, but the patterns of statistical agreement are different, supporting the idea[3] that colder, high-latitude and mountainous edges find no close analogue in the future climate, whereas tropical lowlands will warm beyond the range of current climates.

A critical uncertainty in climate change is the terrestrial biosphere response to climate change feeding back on greenhouse gas concentrations[7,8]. The first generation of coupled carbon–climate models[7], (hereinafter, Earth system models, or ESMs) shows a consistent pattern of carbon loss with warming in the tropics and a carbon gain at mid and high latitudes, although the magnitudes of vary greatly. This dipole pattern is related to the correlation between warming and soil moisture: in the tropics, warming is accompanied by drying and reduced productivity, whereas at mid and high latitudes, warming is accompanied by wetter soils and increased productivity[9]. However, these models share a similar set
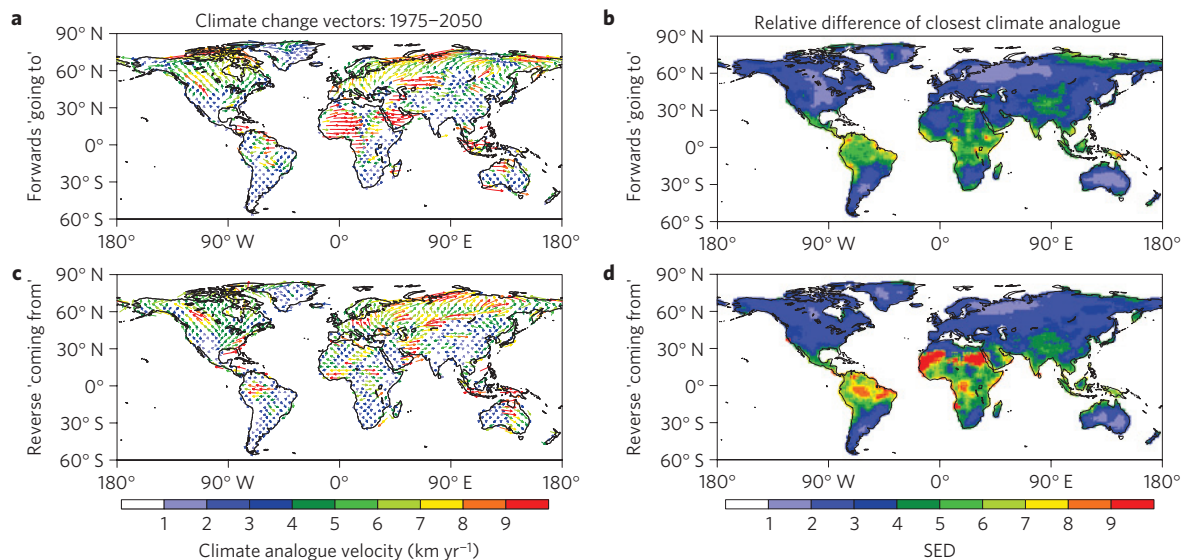
Figure 1 | Climate analogue velocity vectors and statistical difference of analogue climates. Multi-model mean climate change and associated best fit for the forward (where climate is going to) and reverse (where climate is coming from) directions. Arrows for both vectors point in the time-forwards direction. **a,c**, Vectors of mean distance and direction to the best fit climate for the mid-century period (2040–2059) RCP4.5, relative to the baseline historical period (1960–1989). Vector length shows actual distance travelled by the analogue climate over the interval, and the vector colours indicate the mean climate speed. **b,d**, Multi-model ensemble mean error values of the best climate analogue gridcells. Poor fits (large SED values) in **b,d** correspond to areas of disappearing and novel climates, respectively, from ref. 3.

of process representations, and crucially show much greater detail in leaf-level and short-timescale representation than larger-scale and longer-term ecosystem processes such as disturbance and competition that underlie vegetation dynamics; this may be a source of shared bias between models. In particular, dynamic vegetation distributions are not included in most of the ESMs (Table 2). Fuller consideration of carbon loss processes can shift the response away from the dipole pattern: for example, inclusion of permafrost carbon at high latitudes leads to net carbon loss and thus a tripole pattern of carbon loss at low and high latitudes with carbon gain only at mid latitudes[10]. It is therefore useful to seek other conceptual models to understand possible qualitative deviations from the basic dipole pattern.

The application of climate velocities to biome distributions[2] suggests that a similar geographic approach could be useful for understanding the terrestrial carbon response to climate change: if equilibrium vegetation carbon is predominantly controlled by climate, then it will also tend to follow climate velocities. Viewing vegetation carbon as following vectors of climate velocity, the carbon response to climate change becomes analogous to a fluid transport problem: the change in equilibrium carbon equals the product of the spatial carbon gradient and the velocity vector. Fluid dynamics defines a Lagrangian frame of reference as one that travels with the deforming fluid; here I refer to this view of the carbon feedback as the Lagrangian view because it treats carbon as moving with climate analogues rather than responding to changing climate at a fixed location.

This approach suffers from several limitations, which include an inability to consider spatially homogeneous but temporally varying controls on vegetation carbon, such as the direct physiological effect of CO_2, or spatially varying but temporally constant controls, such as soil fertility; an unknown response time for vegetation to adjust to changing climate, which implies that the calculated carbon change is an equilibrium or committed response[11] —actual realized transient changes will differ owing to differing timescales of succession and migration dynamics and carbon gain versus loss processes[12]; the fact that the fidelity of the climate analogue degrades with changing climate and that some future climates have no

Table 1 | List of 21 climate models from the CMIP5 data used in the construction of the historical and RCP4.5 climate change vectors shown in Fig. 1.

Model	Institute
ACCESS1-0	CSIRO-BOM
CCSM4	NCAR
CESM1-BGC	NSF-DOE-NCAR
CESM1-CAM5	NSF-DOE-NCAR
CNRM-CM5	CNRM-CERFACS
GFDL-CM3	NOAA GFDL
GFDL-ESM2G	NOAA GFDL
GISS-E2-R	NASA-GISS
HadGEM2-AO	NIMR-KMA
HadGEM2-CC	MOHC
HadGEM2-ES	MOHC
IPSL-CM5A-LR	IPSL
IPSL-CM5A-MR	IPSL
MIROC-ESM-CHEM	MIROC
MIROC-ESM	MIROC
MIROC5	MIROC
MPI-ESM-LR	MPI-M
MRI-CGCM3	MRI
NorESM1-M	NCC
BCC-CSM1-1	BCC
INM-CM4	INM

analogue in the historical period; and because it is not an actual case of fluid transport, the sets of vectors in Figs 1 and 2 contain discontinuities, for example at continental edges, and thus do not define a smooth vector field. Nonetheless the deliberate simplicity of the Lagrangian approach, by avoiding a mechanistic framework and thus the dependence on the choice of processes included, may allow for qualitative understanding of ESM responses and point toward missing process representation in the more complex and mechanistic set of hypotheses that constitute ESMs.
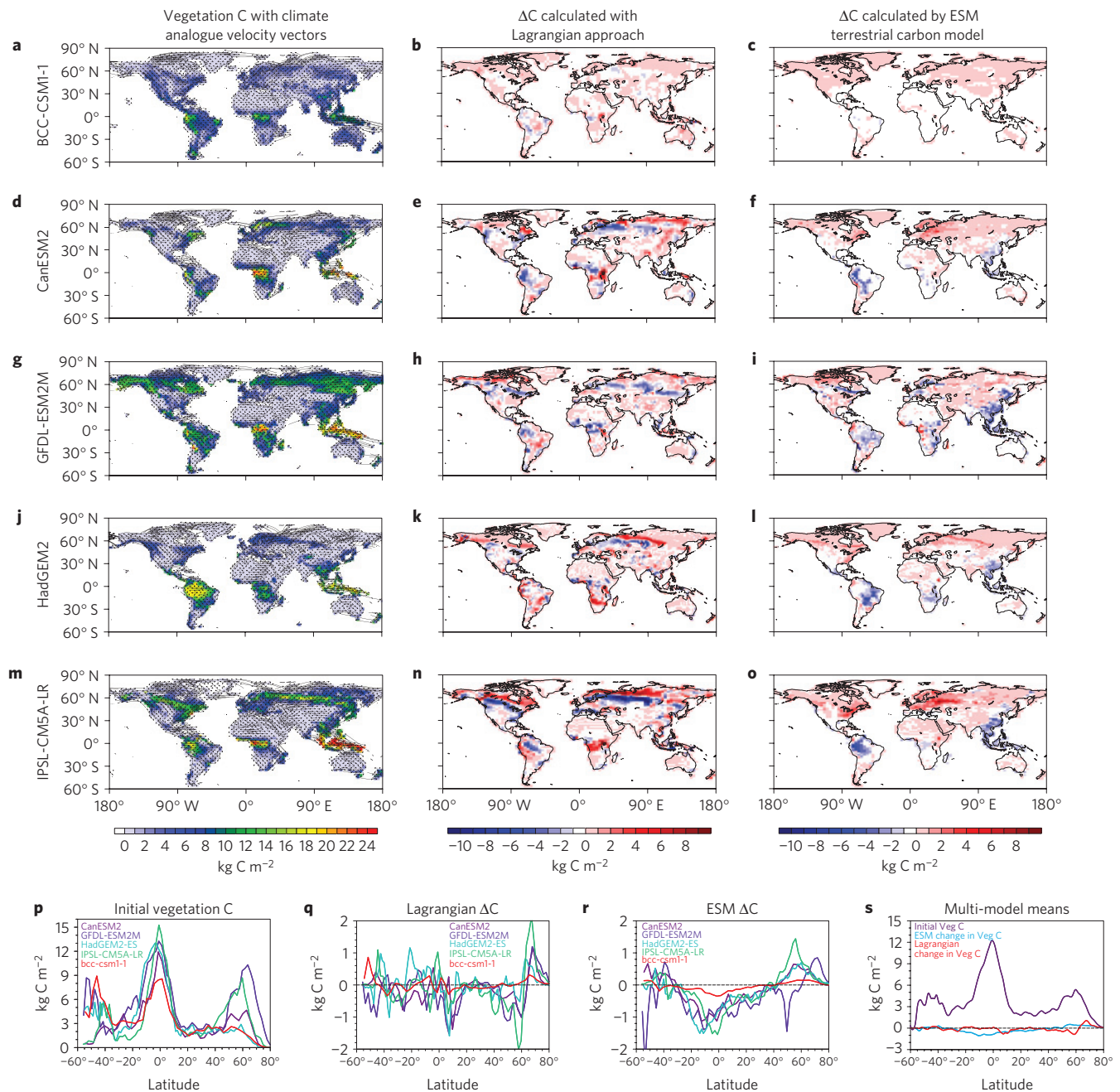
Figure 2 | Lagrangian and ESM terrestrial carbon responses to climate change. Comparison of vegetation carbon changes in the 5 ESMs participating in the CMIP5 esmFdbk2 experiment. Left column (**a**,**d**,**g**,**j**,**m**): climate vectors (in reverse, 'coming from' direction) overlaid onto historical-period mean biomass carbon concentration from each model (kg C m^{-2}). Middle column (**b**,**e**,**h**,**k**,**n**): change in vegetation carbon between the historical (1960–1989) and future (2040–2060 of RCP4.5) climates calculated as a carbon transport by climate velocity approach. Right column (**c**,**f**,**i**,**l**,**o**): change in vegetation carbon between the historical and future climates as calculated by the terrestrial carbon component of the ESMs. **p**–**s**, Zonal mean plots show initial vegetation C (**p**), Lagrangian change in vegetation C (**q**), ESM change in vegetation C (**r**), and multi-model means (**s**).

Many areas of correspondence can be seen between the Lagrangian perspective (Fig. 2, central column) and the ESM responses (Fig. 2, right column). The northern extratropics gain carbon in the ESMs whereas tropical forests lose carbon, following the dipole pattern discussed above. The Lagrangian results differ from the ESMs in two key areas: the southern edge of the boreal forest band and in the tropical forests.

In the boreal forest, the Lagrangian view projects that lower-carbon ecosystems will expand into the current southern boreal forest range, leading to a loss of carbon there. A similar pattern of carbon loss along the southern edge of the boreal forest

appears in only one of the ESMs: the GFDL-ESM2M model, which includes a sophisticated demographic model[13] for prognostic determination of vegetation distributions. The only other ESM in this group with dynamic vegetation distributions, HadGEM2-ES, does not show southern boreal forest carbon loss over this interval, although it may reach such a pattern eventually as it has a long timescale for equilibration[11].

The pattern of carbon losses due to biome transitions accompanying warming in the southern boreal forest has long been proposed by various methods, including coupled biogeography-gap models[14] and remapping of climate zone classifications with changing

Table 2 | Models contributing output for both the historical and future period of the CMIP5 esmFdbk2 experiment used in Fig. 2.

Model	Dynamic vegetation distributions?	Reference
BCC-CSM1-1	No	22
CanESM2	No	23
GFDL-ESM2M	Yes—cohort model	13,24
HadGEM2-ES	Yes—TRIFFID	25,26
IPSL-CM5A_LR	No	27

climate[12] Furrthermore, the current distribution of observed forest carbon density suggests an abrupt transition to lower carbon with warming in this region[15]. Because this is a conceptual rather than mechanistic model, the processes underlying such a shift are undefined, however it is likely that increased mortality agents such as drought, fire and insects will accompany warming[16]. Widespread forest mortality and associated carbon losses have already accompanied unprecedented insect outbreaks in British Columbia[17], which has been linked to warming climate[18]; such insect outbreaks may spread to colder zones of the boreal forests during this century as a result of warming[19]. Ecosystem models that include disturbance suggest that the boreal zone is currently shifting from a carbon sink to a source as a result of fire and other disturbance effects[20].

Integrating the responses regionally, the Lagrangian calculation shows an equilibrium carbon change in the range −27 to −0.17 (mean −12.3) Pg for 40°–60° N, of comparable magnitude to the range of 3.7 to 16 (mean 7.2) Pg gain for 60°–90° N. In contrast, the realized ESM carbon gains are similar for the two bands: in the range −11 to 22 (mean 6.1) Pg for 45°–60° N and in the range 2.3 to 7.8 (mean 5.9) Pg for 60°–90° N. The magnitudes of the equilibrium Lagrangian changes are larger than the ESM changes because the timescales for realizing these changes are longer than the interval considered. Nonetheless, the suggestion that southern carbon losses may offset northern carbon gains due to climate change in the boreal forest underscores the need for ESMs to better include the mechanisms behind these potential losses.

In the tropics, the Lagrangian analysis does not suggest as large a carbon loss as the process-based models do; however, the poor fidelity of the analogue gridcell from which the climate is coming (Fig. 1d) underscores the uncertainty in the tropical forest response to climate change. Because there exist no regions that are moist and hotter than the current tropical forest biome, there is no spatial gradient on which vegetation can shift to accommodate the expected climate change; thus the central assumption of the Lagrangian hypothesis is violated for these regions. Because much of the uncertainty in the tropical C response to warming is determined by vegetation responses to warming[8], this also emphasizes the large uncertainty in the ability of the ESMs to forecast carbon change where novel climates are emerging.

The Lagrangian view presented here defines a simple model for how the terrestrial carbon cycle may respond to climate change. This empirical and equilibrium-based, rather than process-based, hypothesis allows for insights into possible missing mechanisms in current terrestrial models. In particular it suggests that, if the idea of vegetation geographical shifts as a forced response to climate velocity is correct, then the consistently positive mid-latitude carbon change under warming projected by ESMs may highlight a lack of disturbance processes that would lead to carbon loss over the southern boreal domain. Last, by proposing that current carbon spatial gradients along the direction of climate change velocity may be a predictor for future carbon response, this view suggests that focusing ecosystem-monitoring efforts along such gradients may be a strategy for detection of carbon response to climate change.

Methods

Using the historical and Representative Concentration Pathway (RCP) 4.5 climate change scenario from 21 models (Table 1) participating in the Coupled Model Intercomparison Project[21] (CMIP5) project, I calculate the mean and standard deviation of temperature and precipitation for each month in the annual cycle at each gridcell under two time periods: historical (1960–1989), and mid-twenty-first century (2040–2060). Each monthly climatological value is used so that information on the amplitude, shape, and timing of seasonal cycles are included. Then, for each gridcell in one time period, I calculate the standardized Euclidean distance[3] (SED) for every gridcell within a set distance (30°) in the other time period:

$$\text{SED} = \sqrt{\sum_i \left(\frac{\mu_{i,\text{ref}} - \mu_{i,\text{mod}}}{\sigma^2_{i,\text{ref}}}\right)_2}$$

where i is the index of climate variables used (24 total: 12 monthly mean temperature and 12 monthly mean precipitation values), $\mu_{i,\text{ref}}$ and $\mu_{i,\text{mod}}$ are the means of climate variable i, and $\sigma_{i,\text{ref}}$ is the standard deviation (across multiple years and ensemble members for a given model) of climate variable i in the reference period. The gridcell that corresponds best is that which minimizes the SED error function between the two time periods. The vectors and their corresponding minimum error were calculated separately for each model, spanning multiple ensembles where available, then averaged to define a multi-model ensemble-mean set of climate change vectors and associated minimum error (Fig. 1). The climate speed is calculated as the great-circle length of the climate analogue distance vector divided by the time interval between the midpoints of the two periods analysed. The multi-model mean climate analogue velocity vectors are calculated by regridding the calculate change in latitude and longitude from each model using bilinear interpolation to a uniform 1-degree grid, and then averaged to 3-degree resolution for plotting.

The Lagrangian carbon change is calculated as:

$$\frac{\partial C}{\partial t} = -\left(u\frac{\partial C}{\partial x} + v\frac{\partial C}{\partial y} \right)$$

where C is the equilibrium vegetation carbon, u and v are the components of climate analogue velocity, and $\partial C/\partial x$ and $\partial C/\partial y$ are the spatial gradients in vegetation carbon under the historical climate. I focus on vegetation carbon here as it is likely to be both more directly controlled by climate, and more rapidly responsive to climate changes than soil carbon; however an analogous calculation could be performed for soil carbon.

For the Lagrangian carbon change calculation, I calculate the vectors separately for each of the 5 models participating in the 'esmFdbk2' of the CMIP5 experimental protocol, which uses historical and RCP4.5 greenhouse gas concentrations for radiative calculations but constant pre-industrial CO_2 for physiological effects on vegetation (experiment 5.5.2 in ref. 21; Supplementary Fig. S3 also shows results for the 1% CO_2 increase/year esmFdbk1 experiment, experiment 5.5.1 in ref. 21), and calculate the carbon change over the period 1975–2050 using the vectors calculated in the 'coming from' direction from that model and the model-calculated biomass C stocks at 1975. Before the transport calculation, a smoothing step (3 × 3 gridcell moving means) is applied on both the C gradients and the u and v velocity vectors to reduce the high-frequency variation. For the transport calculation, a constant velocity is used with 5-year timesteps. As a test of the assumptions in the transport calculation itself, Supplementary Fig. S4 shows the carbon changes calculated as a simple substitution of carbon from the best analogue climate, with qualitatively similar results. The transport calculation itself is Eulerian; I use the term Lagrangian in the paper only to distinguish the transport hypothesis from the fixed reference frame of the ESM prognostic carbon cycle. I compare this carbon transport change directly to the change in biomass carbon projected across the interval from 1975 to 2050 by each ESM during the experiment. The vectors shown in Fig. 2 are also calculated as in Fig. 1.

References

1. Davis, M. B. & Shaw, R. G. Range shifts and adaptive responses to quaternary climate change. *Science* **292,** 673–679 (2001).
2. Loarie, S. R. *et al*. The velocity of climate change. *Nature* **462,** 1052–1055 (2009).
3. Williams, J. W., Jackson, S. T. & Kutzbach, J. E. Projected distributions of novel and disappearing climates by 2100 AD. *Proc. Natl Acad. Sci. USA* **104,** 5738–5742 (2007).
4. Dobrowski, S. Z. *et al*. The climate velocity of the contiguous United States during the 20th century. *Glob. Change Biol.* **19,** 241–251 (2012).
5. Ackerly, D. D. *et al*. The geography of climate change: Implications for conservation biogeography. *Divers. Distrib.* **16,** 476–487 (2010).
6. Veloz, S. *et al*. Identifying climatic analogs for Wisconsin under 21st-century climate-change scenarios. *Climatic Change* **112,** 1037–1058 (2012).
7. Friedlingstein, P. *et al*. Climate–carbon cycle feedback analysis: Results from the C4MIP model intercomparison. *J. Clim.* **19,** 3337–3353 (2006).

8. Booth, B. B. B. *et al.* High sensitivity of future global warming to land carbon cycle processes. *Environ. Res. Lett.* **7,** 024002 (2012).

9. Fung, I., Doney, S., Lindsay, K. & John, J. Evolution of carbon sinks in a changing climate. *Proc. Natl Acad. Sci. USA* **102,** 11201–11206 (2005).

10. Koven, C. D. *et al.* Permafrost carbon-climate feedbacks accelerate global warming. *Proc. Natl Acad. Sci. USA* **108,** 14769–14774 (2011).

11. Jones, C., Lowe, J., Liddicoat, S. & Betts, R. Committed terrestrial ecosystem changes due to climate change. *Nature Geosci.* **2,** 484–487 (2009).

12. Smith, T. M. & Shugart, H. H. The transient response of terrestrial carbon storage to a perturbed climate. *Nature* **361,** 523–526 (1993).

13. Shevliakova, E. *et al.* Carbon cycling under 300 years of land use change: Importance of the secondary vegetation sink. *Glob. Biogeochem. Cycles* **23,** GB2022 (2009).

14. Sykes, M. T. & Prentice, I. C. Boreal forest futures: Modelling the controls on tree species range limits and transient responses to climate change. *Wat. Air Soil Pollut.* **82,** 415–428 (1995).

15. Scheffer, M., Hirota, M., Holmgren, M., Van Nes, E. H. & Chapin, F. S. Thresholds for boreal biome transitions. *Proc. Natl Acad. Sci. USA* **109,** 21384–21389 (2012).

16. Anderegg, W. R. L., Kane, J. M. & Anderegg, L. D. L. Consequences of widespread tree mortality triggered by drought and temperature stress. *Nature Clim. Change* **3,** 30–36 (2013).

17. Kurz, W. A. *et al.* Mountain pine beetle and forest carbon feedback to climate change. *Nature* **452,** 987–990 (2008).

18. Macias Fauria, M. & Johnson, E. A. Large-scale climatic patterns and area affected by mountain pine beetle in British Columbia, Canada. *J. Geophys. Res.* **114,** G01012 (2009).

19. Bentz, B. J. *et al.* Climate change and bark beetles of the Western United States and Canada: Direct and indirect effects. *BioScience* **60,** 602–613 (2010).

20. Hayes, D. J. *et al.* Is the northern high-latitude land-based CO_2 sink weakening? *Glob. Biogeochem. Cycles* **25,** GB3018 (2011).

21. Taylor, K. E., Stouffer, R. J. & Meehl, G. A. An overview of CMIP5 and the experiment design. *Bull. Am. Meteorol. Soc.* **93,** 485–498 (2012).

22. Ji, J., Huang, M. & Li, K. Prediction of carbon exchanges between China terrestrial ecosystem and atmosphere in 21st century. *Sci. China* **51,** 885–898 (2008).

23. Arora, V. K. *et al.* Carbon emission limits required to satisfy future representative concentration pathways of greenhouse gases. *Geophys. Res. Lett.* **38,** L05805 (2011).

24. Dunne, J. P. *et al.* GFDL's ESM2 global coupled climate-carbon Earth System Models Part I: Physical formulation and baseline simulation characteristics. *J. Clim.* **25,** 6646–6665 (2012).

25. Cox, P. M. in *Description of the TRIFFID Dynamic Global Vegetation Model* (Hadley Center Technical Note, Vol. 24, UK Met Office, 2001).

26. Jones, C. D. *et al.* The HadGEM2-ES implementation of CMIP5 centennial simulations. *Geosci. Model Dev.* **4,** 543–570 (2011).

27. Krinner, G. *et al.* A dynamic global vegetation model for studies of the coupled atmosphere-biosphere system. *Glob. Biogeochem. Cycles* **19,** GB1015 (2005).

Acknowledgements